

The One RING : a Robotic Indoor Navigation Generalist

Ainaz Eftekhari^{1,2} Luca Weihs² Rose Hendrix² Ege Caglar¹
Jordi Salvador² Alvaro Herrasti² Winson Han² Eli VanderBil²
Aniruddha Kembhavi^{1,2} Ali Farhadi^{1,2} Ranjay Krishna^{1,2} Kiana Ehsani^{*2}
Kuo-Hao Zeng^{*2}
¹University of Washington
²Allen Institute for AI

one-ring-policy.allen.ai

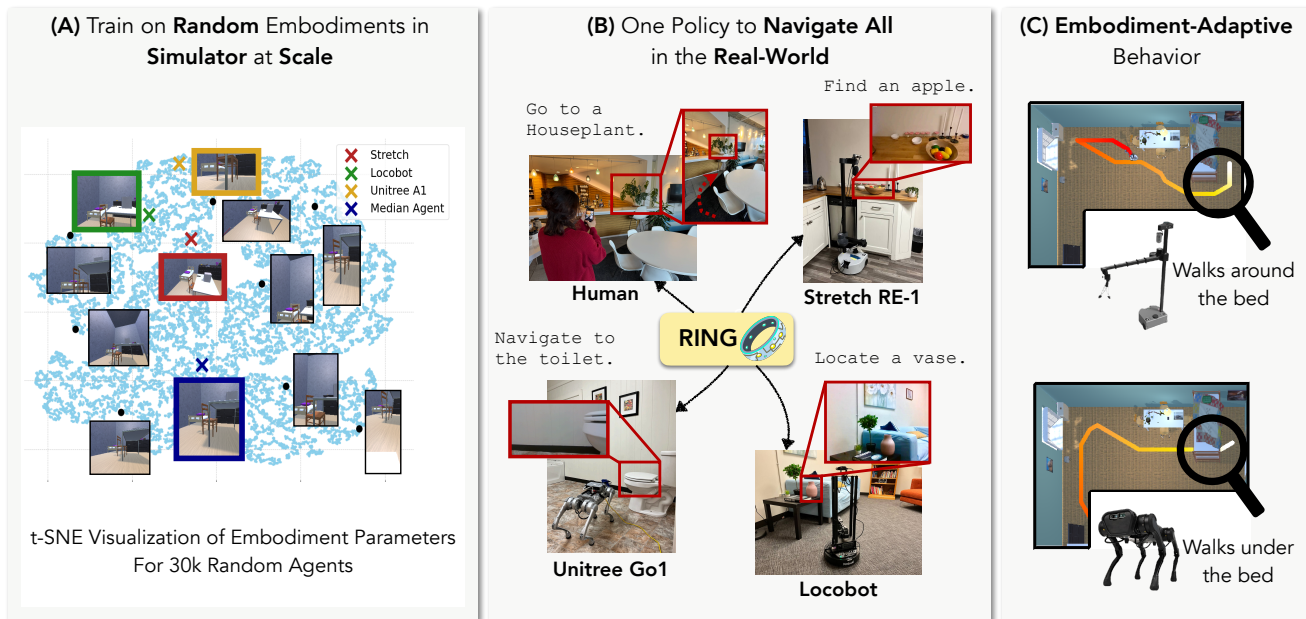


Figure 1. (A) We train on *one million* randomly generated embodiments in simulation varying camera configurations, body size, and rotation pivot point. The plot shows the t-SNE visualization of embodiment parameters $\mathbf{c}_e \in \mathbb{R}^{19}$ for 30k random agents and three specific robots (robots are for visualization—we do not train on any real robot embodiment parameters). Egocentric views from the first camera are shown for 10 sample agents. (B) Our trained policy transfers zero-shot to a wide range of embodiments in the real-world including Stretch RE-1, LoCoBot, and Unitree Go1, as well as a human embodiment. (C) The RING policy displays embodiment-adaptive behavior, adjusting its navigation strategy based on its embodiment.

Abstract

Modern robots vary significantly in shape, size, and sensor configurations used to perceive and interact with their environments. However, most navigation policies are embodiment-specific; a policy learned using one robot’s configuration does not typically gracefully generalize to another. Even small changes in the body size or camera view-point may cause failures. With the recent surge in custom

hardware developments, it is necessary to learn a single policy that can be transferred to other embodiments, eliminating the need to (re-)train for each specific robot. In this paper, we introduce RING (**R**obotic **I**ndoor **N**avigation **G**eneralist), an embodiment-agnostic policy, trained solely in simulation with diverse randomly initialized embodiments at scale. Specifically, we augment the AI2-THOR simulator with the ability to instantiate robot embodiments with controllable configurations, varying across body size,

rotation pivot point, and camera configurations. In the visual object-goal navigation task, RING achieves robust performance on real unseen robot platforms (Stretch RE-1, LoCoBot, Unitree’s Go1), achieving an average of 72.1% and 78.9% success rate across 5 embodiments in simulation and 4 robot platforms in the real world.

1. Introduction

Robot embodiments are diverse and are constantly evolving to better suit new environments and tasks. This range in body configurations—differences in size, shape, wheeled or legged locomotion, and sensor configurations—not only shapes how robots perceive the world but also how they act in it. A robot with a wide field of view (FoV) or multiple cameras can scan its surroundings quickly, while one with a narrower view might need to more actively explore a room. A small robot can squeeze through tight spaces, a low-profile one can duck under furniture, and a larger robot may need to follow more conservative routes. The influence of embodiment on behavior means a policy trained on one design, or even several, often does not perform well out of domain [62].

There has been progress towards scalable cross-embodiment training [34, 45] and in developing general-purpose navigation policies [13, 42, 43, 56]. While these methods demonstrate some transfer to unseen embodiments, they require construction of topological maps or graphs and suffer performance degradation with relatively small changes in embodiment (*e.g.*, camera position modification on the same robot). Potentially, this is due to these methods relying on the small amount of real-world data available in public datasets—only around 20 embodiments in total. This highlights the need for a more comprehensive solution that reliably covers the wide range of possible embodiments without retraining or additional adaptation.

We introduce RING, a **R**obotic **I**ndoor **N**avigation **G**eneralist. RING is trained exclusively in simulation, without any use of real-world robot embodiments. In other words, all robot platforms we evaluate on (*i.e.*, Stretch RE-1, LoCoBot, Unitree’s A1) are *unseen* by RING during training. We leverage simulation to randomly sample **1 Million** agent body configurations, varying the robot’s camera parameters, collider sizes, and center of rotation. Concretely, each embodiment consists of a collider box of varying dimensions and cameras with randomized FoV and dimensions, placed randomly within the collider box. Fig. 1-A shows a t-SNE [46] visualization of body parameters for 30k random agents in our generated data.

Our method is inspired by the recent success in real-world experiments while training at large-scale only in simulation [17, 24, 62]. Simulation training is able to benefit from the vast scale of scenes (150k ProcTHOR

houses [12]) and objects (40k+ annotated 3D objects from Objaverse [11]) in the AI2-THOR simulator. Extensive domain randomization on visual observations and the use of pre-trained visual encoders then allows simulation-trained policies to bridge the sim-to-real gap. We follow the training procedure outlined in FLaRe [24], first training our policy on expert trajectories collected from 1M randomized embodiments and subsequently fine-tuning it with on-policy reinforcement learning (RL) within the simulator.

Our results demonstrate generalization to *truly unseen embodiments*. RING generalizes to diverse real-world embodiments without any adaptation, despite being trained exclusively in simulation without access to the real robot configurations. We evaluate our policy in a zero-shot setting across a variety of embodiments, including the Stretch RE-1, LoCoBot, Unitree’s A1, and even “Navigation Assistants”, wherein a human user captures ego-centric observations on their phone and prompt RING policy to predict actions to navigate. RING achieves 72.1% and 78.9% success rate on average, outperforming the best baseline significantly, both in simulation and the real-world.

We highlight three key characteristics of RING: **1)** it displays zero-shot generalization to unseen embodiments, keeping a consistently high performance (Sec. 4.1); **2)** it can zero-shot transfer to the real-world without any adaptation or real-world-specific finetuning. (Sec. 4.2); **3)** it can be adapted to an embodiment-specialized policy with even better performance with minimal finetuning (Sec. 4.3); and **4)** at inference, it dynamically adjusts its behavior based on the embodiment (Sec. 4.4, Fig. 6). RING can be directly deployed to navigate any robot platform, is easy to install, and is ready for use by researchers in the community. We will release our pretrained models, generated data, and training code.

2. Related work

Cross-embodiment. Cross-embodiment training has received substantial attention from the research community. Arguably the most representative of a large body of recent work [3, 7, 13, 14, 19, 21, 23, 25, 28, 30, 33, 47, 52, 53, 56, 60], Open-X-Embodiment (OXE) [9] is the fruit of a large collaboration to cover many robotic tasks, with special emphasis in manipulation. Its usage in RT-X results in a notable performance gain in emergent skill evaluations in comparison to RT-2 [5]. Despite the 1.5 million trajectories across 22 embodiments present in their dataset, the enormous cost of data collection in the real world makes further scaling challenging. CrossFormer [13] trains a transformer-based policy on 900k trajectories across 30 robots, including a subset of OXE, navigation data from GNM [42], manipulation data from DROID [27], and additional collected data. Due to the relatively sparse amount of embodiments observed during training and the target low-level control, it

does not generalize to unseen embodiments. GET-zero [36] focuses on dexterous manipulation, and proposes to inform the policy with the structure of the embodiment via a connectivity graph to bias the attention. In contrast, we generate an arbitrarily large amount of embodiments for training our policy, enabling zero-shot deployment to new embodiments without accessing the embodiment structure.

Foundational navigation policies. Following the success in recent developments for point-goal navigation [50], locomotion [4, 39, 41], agile control [51], exploration [6, 55, 57], and social navigation [37], comparable results in more nuanced tasks like semantic or object-goal navigation (ObjectNav) [2, 15, 26, 31, 40, 48, 58, 61] remain elusive due to a lack of efficient exploration and semantic understanding capabilities. Recently, with powerful pretrained foundational vision models [35, 63] and large-scale procedurally generated virtual environments [11], notable progress in end-to-end ObjectNav policy learning *for specific embodiments* has been achieved by means of imitation learning (IL) from shortest-path trajectories [17], RL [62], or combinations thereof [24]. In image-goal navigation, NoMaD [44], which extends ViNT [43], uses a diffusion policy to control a single embodiment. With the same goal in mind, GNM [42] trains navigation policies across 6 embodiments using IL. In contrast, our policy benefits from finetuning with RL, improving resilience to compounding errors. Additionally, thanks to training with large-scale randomized embodiments in simulation, RING learns a single policy to navigate *any* embodiment, generalizing to *truly* unseen robot platforms in the real world. Furthermore, NoMaD, ViNT, GNM, and Mobility VLA [54] all require topological map or graph reconstruction for high-level planning, whereas our policy is fully end-to-end and explores novel scenes without an explicit map. While several efforts [1, 32, 59] focus on learning embodiment-agnostic policies using LLMs or VLMs, they address only short-horizon navigation tasks and perform single-step predictions. In contrast, RING models temporal information through a transformer decoder.

3. RING

With the growing diversity of robots used in research labs and real-world applications, there remains a need for a policy that can operate a wide range of embodiments and transfer, in a zero- or few-shot manner, to unseen robots. We introduce RING, a generalist policy for indoor visual navigation that *learns from a broad spectrum of embodiments, trained exclusively in simulation, without any direct use of actual robot embodiments*. We show that training on an extensive range of $\sim 1\text{M}$ random embodiments results in a robust navigation policy, enabling zero-shot transfer to unseen real-world robot embodiments. To train RING, we define

Parameters	Training Range
Collider Size ($\alpha_x, \alpha_y, \alpha_z$)	$[0.2, 0.5]$, $[0.3, 1.5]$, $[0.2, 0.5]$
Rotation Center (o_x, o_y, o_z)	$[-\alpha_x/2, \alpha_x/2]$, $[-\alpha_y/2, \alpha_y/2]$, $[-\alpha_z/2, \alpha_z/2]$
Vertical FoV (cam1, cam2)	$[40, 100]$, $[40, 100]$
Horizontal FoV (cam1, cam2)	$[40, 120]$, $[40, 120]$
Camera Pitch (cam1)	$[-20, 40]$
Camera Pitch (cam2)	$[-20, 60]$
Camera Yaw (cam1, cam2)	always 0, $[0, 360]$
Camera Position (x) (cam1, cam2)	$[-\alpha_x/2, \alpha_x/2]$, $[-\alpha_x/2, \alpha_x/2]$
Camera Position (y) (cam1, cam2)	$[0.3, \alpha_y]$, $[0.3, \alpha_y]$
Camera Position (z) (cam1, cam2)	$[-\alpha_z/2, \alpha_z/2]$, $[-\alpha_z/2, \alpha_z/2]$
RGB dimensions (H, W)	$[112, 448]$, $[112, 448]$

Table 1. **Random Embodiment Parameters.** We generate 1M different embodiments sampled from the ranges above.

the space of random embodiments (Sec. 3.2), enable generation of expert trajectories for random embodiments in simulation (see Appendix 7), and use state-of-the-art architecture designs (Sec. 3.3) to train with a combination of IL and RL methods (Sec. 3.4).

3.1. Problem formulation

Learning a navigation policy across multiple embodiments is a multi-task robotic problem. We define the space of possible embodiments as \mathcal{E} , where each embodiment $e \in \mathcal{E}$ is characterized by a configuration vector \mathbf{c}_e , which includes parameters such as camera settings, agent collider size, center of rotation, etc. Each task can be modeled as a Partially Observable Markov Decision Process (POMDP), denoted as $(\mathcal{S}, \mathcal{A}, \mathcal{E}, \mathcal{O}_e, \mathcal{T}_e, R, \mathcal{L}, P(s_0), \gamma)$, where \mathcal{S} and \mathcal{A} are the state and action spaces. The observation space \mathcal{O}_e varies across embodiments due to differences in camera parameters and sensor configurations. The observation at time t for embodiment e , $o_t^e = \mathcal{O}_e(s_t, \mathbf{c}_e)$, is a function of both the state s_t and embodiment parameters \mathbf{c}_e . Given an action a_t , the next state follows the transition dynamics $s_{t+1} \sim \mathcal{T}_e(s_{t+1}|s_t, a_t, \mathbf{c}_e)$, which depends on the embodiment, as different embodiments interact with the environment in distinct ways (due to variations in collider size and center of rotation). Fig. 2 shows example trajectories from two different embodiments starting at the same location and following the same sequence of actions. They have distinct visual observations and follow different transition dynamics—one agent moves under the table, while the other collides with it. Except where otherwise specified, we assume that all embodiments share the same discrete action space $\{\text{MoveBase}(\pm 20\text{cm}), \text{RotateBase}(\pm 6^\circ, \pm 30^\circ), \text{Done}\}$, and use robot-specific low-level controllers to execute these actions during deployment.

3.2. Embodiment randomization at scale

Domain randomization [8] is a class of methods in which policies are trained across a wide range of simulated *environmental* parameters; the aim is to enable robustness to unseen environments. Our approach is complementary yet orthogonal; we apply embodiment randomization to train

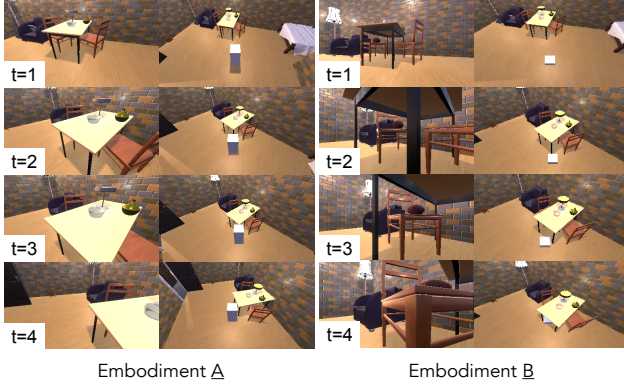


Figure 2. **Different embodiments exhibit different behaviors.** For each embodiment in these sample trajectories, the left column shows the first-person view from the main camera and the second one a third-person view of the agent –white boxes indicate the robot colliders. Embodiment A (shown on the left) has a bigger body size compared to Embodiment B (shown on the right). As a result, B can go under the table to get to the chair but A collides with the table and has to go around.

policies on a diverse set of *robot body* parameters, enabling robust deployment to unseen real-world robots.

We model the body of the agent as an invisible collider box in the AI2-THOR [29] simulator. Each agent can have 1 or 2 RGB cameras placed at a random pose within the collider box. Parameters corresponding to both the body and the cameras are sampled randomly from the ranges specified in Table 1. We also modify the process of generating expert trajectories to account for the diversity of embodiments, for details see Appendix 7. Below, we detail the parameters varied in our embodiment randomization.

Collider size ($\alpha_x, \alpha_y, \alpha_z$). The agent’s body is modeled as a collider box. We use three scale factors ($\alpha_x, \alpha_y, \alpha_z$) to scale the box along x, y, z axis. We sample α_x and α_y uniformly from the range $[0.2, 0.5]$ m and sample α_z (the height of the agent) from the range $[0.3, 1.5]$ m. These ranges adequately capture the variability among most robots.

Rotation center (o_x, o_y, o_z). These coordinates define the agent’s pivot point. While this center is typically near $(0,0)$, it can vary across different robots. We sample o_x from the range $[-\frac{\alpha_x}{3}, \frac{\alpha_x}{3}]$ and o_y from the range $[-\frac{\alpha_y}{3}, \frac{\alpha_y}{3}]$, with the sampling ranges determined by the collider size.

Camera parameters. Each agent is equipped with two RGB cameras placed within the collider box. We randomize several camera parameters, including position, rotation, FoV, and aspect ratio. The sampling ranges for these parameters are shown in Table 1. While the first camera always faces forward, the second camera can rotate up to 360° in z -axis, enabling it to face forward, to the sides, or backward.

For visualization purposes, we define an embodiment configuration vector $\mathbf{c}_e \in \mathbb{R}^{19}$ for each embodiment, rep-

resenting the camera and body parameters. Fig. 1-A shows a t-SNE visualization of the vectors \mathbf{c}_e for 30k of our random embodiments, along with the corresponding vectors for Stretch RE-1, LoCoBot, and Unitree A1. The figure also includes the egocentric view from the first camera for 10 random embodiments, and the three robots. This demonstrates that our randomization spans a wide range of possible embodiments, covering the real-world robot platforms of interest. In total, we gather **1M** trajectories across 50k houses, each with a randomly sampled embodiment (more details in Appendix 10).

3.3. Architecture

With this rich dataset of expert trajectories for random embodiments, a deep, high-capacity architecture is essential to learn a robust policy. In this section, we introduce our model architecture, shown in Fig. 3. At each timestep, RING uses N RGB images (one per camera) and a language instruction l to predict an action distribution over a discrete action space. To account for different dimensions, we pad the RGB observations to make them square and resize them to 256×256 before feeding them to the model. RING’s architecture, inspired by PoliFormer [62], consists of a Visual Encoder, a Goal Encoder, a Transformer State Encoder, and a Causal Transformer Decoder with a linear actor-critic head. The Visual and Goal Encoders are frozen pre-trained models (a ViT and a language model, respectively) that encode the RGB observations and instruction l into visual and goal token embeddings. Projections of these embeddings, along with a special STATE token vector, are stacked along the token axis and processed by the multi-layer Transformer State Encoder, which summarizes the observations at each timestep as the state embedding corresponding to the STATE token. Finally, the Causal Transformer Decoder performs explicit memory modeling over time, producing the current belief by causal attention on the state embeddings stacked along the temporal axis. The linear actor-critic head further predicts action logits over the action space as well as a value estimate. We provide more details about the architecture in the Appendix 9.

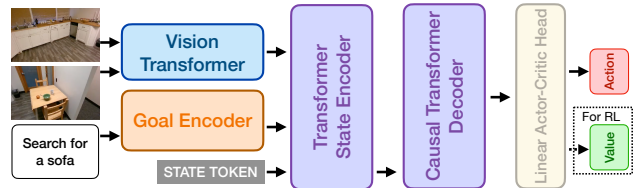


Figure 3. **Our RING model architecture.** It accepts visual observations and a language instruction as inputs and predicts an action to execute. At RL finetuning, RING also predicts a value estimate.

3.4. Training Paradigm

Recently, SPOC [17] showed that training policies with Behavior Cloning on large-scale expert trajectories in simulation leads to policies that effectively generalize to the real world. FLaRe [24] further introduced a robust and scalable method for finetuning such pretrained policies with On-policy Reinforcement Learning. RL finetuning introduces error recovery behaviors and mitigates the compounding errors typically encountered in imitation learning, leading to a substantial performance boost. We adopt the same recipe of first pretraining our policy on expert trajectories collected from randomized embodiments (Sec. 3.2), followed by finetuning with on-policy RL using the randomized embodiments in the AI2-THOR simulator [29].

Large-scale imitation learning with random embodiments. We train our policy using the architecture outlined in Sec. 3.3 on the collected trajectories. At each time step, the linear actor-critic head in Causal Transformer Decoder predicts the action logits. The cross-entropy loss is computed between the logits π^t and the expert action. At training, we use a batch size of 240 trajectories and each trajectory has a temporal context window of 100 steps. We train our model on $8 \times$ H100 GPUs (80 GB memory per GPU) using the AdamW optimizer with a learning rate of $2 \cdot 10^{-4}$ for 80k iterations.

RL finetuning with random embodiments. Following the training recipe in FLaRe [24], we further perform a large-scale RL finetuning using AllenAct [49] on the randomized embodiments in simulation. Our training includes 1M random embodiments, 50k procedurally generated PROCTHOR houses [12] with ~ 40 k annotated 3D objects [18]. RL finetuning is specifically important for the policy to learn to navigate a diverse set of embodiments through trial-and-error. In particular, as the RING policy lacks explicit information about its embodiment, it must implicitly infer it, which requires extensive exploration and trial-and-error. We use DD-PPO with 64 parallel environments and 128 rollout steps across 4 machines (each with $8 \times$ H100 GPUs) using the AdamW optimizer with a learning rate of $2 \cdot 10^{-5}$ for 40M training steps. Following FLaRe, we turn off the entropy term in the PPO loss to avoid catastrophic forgetting. For fair comparison, we use the reward function of [12],

$$r_t = \max(0, \min \Delta_{0:t-1} - \Delta_t) + s_t - \rho, \quad (1)$$

where $\min \Delta_{0:t-1}$ denotes the minimum L2 distance between the agent and any target object up to time $t - 1$, Δ_t is the most recent L2 distance, s_t is a success reward, and ρ denotes the step penalty of 0.01 to encourage the policy to finish the task efficiently. The agent must issue `DONE` to indicate that it has found the target object to get the success reward $s_t = 10$, otherwise $s_t = 0$.

4. Experiments

Our experiments show that RING operates effectively across a wide range of embodiments, including actual robots (*Stretch RE-1*, *LoCoBot*, and *Unitree Go1*) and human evaluation with *Navigation Assistants*, despite being trained exclusively in simulation **without** any direct exposure to real robot embodiments. Our key results are:

1. RING generalizes **zero-shot** to 4 *truly* unseen embodiments, despite never being trained on them, and achieves state-of-the-art performance across multiple benchmarks (Sec. 4.1).
2. Our policy, trained solely in simulation on randomized embodiments, transfers directly to the **real-world**, on 3 real robots and navigation assistants (human evaluation). (Sec. 4.2).
3. RING can be easily adapted to **embodiment-specialized** policies with minimal finetuning. It achieves better performance on each specific robot (Sec. 4.3).
4. RING shows **embodiment-adaptive behavior**, adjusting its strategies based on the agent’s body (Sec. 4.4).
5. We present ablation studies and explore finetuning with collision penalties to enable the policy to take more conservative actions (Sec. 4.5).

4.1. RING generalizes zero-shot to unseen embodiments

In this section, we perform zero-shot evaluations of all policies on four robot embodiments: Stretch RE-1 (with 1 or 2 cameras), LoCoBot, and Unitree A1 in simulation.

Baselines. For our baselines, we selected prior works in both imitation learning (IL) and reinforcement learning (RL). Each baseline is trained on a specific embodiment and evaluated in a zero-shot setting on four different embodiments. SPOC [16] is a supervised IL baseline trained on shortest-path expert trajectories in AI2-THOR. PoliFormer [62] is a state-of-the-art transformer-based policy in object goal navigation, trained from scratch using RL. FLaRe [24] is a approach for efficient policy finetuning that combines IL and RL. Specifically, SPOC [17] is trained with IL on Stretch RE-1 using 100k expert trajectories; SPOC-2.3M is trained on more expert trajectories; PoliFormer [62] is trained from scratch on each embodiment individually over 300M RL steps; and FLaRe [24] finetunes SPOC on Stretch RE-1 with an additional 20M RL steps.

Experimental Details. RING is first trained with IL on 1M expert trajectories collected from randomized embodiments in simulation, followed by finetuning with RL for an additional 40M steps on the randomized embodiments (examples shown in Fig. 1-A and Fig. 2). *Note that all four target embodiments were unseen during training, and information on embodiment is not provided during evaluation.* We evaluate on the navigation benchmark in CHORES- \S [17], a

Model	Loss	Train Embodiment	Benchmark Embodiment					Average
			Stretch	Stretch (Nav Cam)	Stretch (Factory Config)	LoCoBot	Unitree A1	
SPOC [17]	IL only	Stretch	57.0 (38.1)*	37.9 (19.0)	33.0 (19.3)	16.2 (5.4)	2.1 (1.6)	29.2 (16.7)
SPOC-2.3M			60.0 (30.3)*	37.5 (17.9)	46.0 (19.4)	24.0 (7.9)	10.0 (5.2)	35.5 (16.1)
POLIFORMER [62]	RL only	Stretch	81.0 (58.1)*	65.0 (35.5)	47.5 (25.6)	27.5 (14.8)	42.6 (25.1)	52.7 (31.8)
		LoCoBot	56.0 (32.9)	56.5 (34.7)	52.0 (27.7)	61.5 (44.7)*	50.5 (34.2)	55.4 (34.9)
		Unitree A1	40.0 (25.2)	39.0 (22.5)	35.5 (20.9)	30.0 (17.4)	55.3 (48.2)*	40.0 (26.8)
FLARE [24]	IL + RL	Stretch	82.0 (63.5)*	55.5 (37.9)	38.0 (19.6)	21.5 (10.9)	27.0 (15.1)	44.8 (29.4)
RING-ZERO-SHOT	IL + RL	RING-Random	76.0 (55.9)	74.0 (52.5)	72.0 (52.7)	66.5 (45.3)	72.0 (58.6)	72.1 (53.0)

Table 2. **Zero-shot Results.** RING shows 0-shot generalization on 4 unseen embodiments. Stretch RE-1 and LoCoBot are evaluated on the CHORES-S [17] ObjectNav benchmark (Unitree A1 is evaluated on a different benchmark which accounts for the agent’s lower height). “Stretch” without further qualification refers to the 2-camera variation on an RE-1 platform, as in [17]. All previous methods drastically fail to generalize to embodiments other than their training. Gray* numbers are evaluated on the training embodiment, otherwise evaluated zero-shot on an unseen embodiment.

simulation benchmark for household robot with 200 tasks across 200 scenes. For Unitree A1, we create a new, similar benchmark with 200 tasks adjusted for the robot’s lower height to ensure that all targets are feasible.

Results. Table 2 presents the zero-shot evaluation of all policies across four embodiments. We compare *Success Rate* and *Success Weighted by Episode Length (SEL [15])*, a metric measuring efficiency. The results indicate that all single-embodiment baselines struggle to generalize effectively to new embodiments, with performance declining as embodiment differences increase. For example, SPOC trained on the Stretch RE-1 with two cameras shows a gradual decrease in performance as the evaluation embodiment diverges from left to right on the top row in Table 2. It is worst when evaluated on the Unitree A1, which has a substantial height difference. In contrast, RING exhibits strong generalization across all embodiments, despite not being trained on any of them, achieving an average absolute improvement of 16.7% in Success Rate. In some cases, it outperforms the baseline trained on the target embodiment: PoliFormer trained on LoCoBot (61.5 → 68.5) and Unitree A1 (55.3 → 72.0). This shows that RING benefits from training across random embodiments at scale, leading to a more effective navigation policy which even outperforms some embodiment-specialized policies (more detail on real robot experiments in Appendix 6.1).

4.2. RING transfers to real-world embodiments despite being purely trained in simulation

Robot Evaluation We zero-shot evaluate our policy on 3 unseen robots in a real-world apartment. All evaluations are performed directly in a large-scale apartment (Fig. 4), without any further adaptation or real-world-specific finetuning. We used the same evaluation set of 15 tasks for LoCoBot [10, 12, 62] (3 different starting poses with 5 different targets), and 18 tasks for Stretch RE-1 [17, 24, 62] (3 different starting poses with 6 different goal specifications), respectively. We create a new evaluation set for Unitree Go1

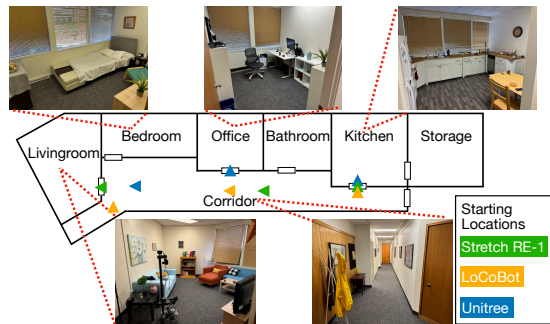


Figure 4. **Real Evaluation Environment.** Our real-world evaluations are performed in a multi-room apartment with a long corridor, shown here with the three starting locations for three different robots’ evaluations.

Model	Train Embodiment	Eval Embodiment			
		Stretch	Stretch (FC)	LoCoBot	Unitree Go1
ProcTHOR [12]	LoCoBot	-	-	26.7	-
Phone2Proc [10]	LoCoBot	-	-	66.7	-
SPOC [16]	Stretch	50.0	-	-	-
POLIFORMER [62]	Stretch	83.3	33.3	-	-
	LoCoBot	-	-	80.0	-
	Unitree Go1	-	-	-	41.7
FLARE [24]	Stretch	94.4	-	-	-
RING-ZERO-SHOT	RING-Random	83.3	72.2	80.0	80.0

Table 3. **Real-world Results.** RING transfers zero-shot to the real-world without any finetuning. Gray numbers are evaluated on same embodiment as their training. RING achieves 78.9% success rate on average across 4 real-world robots.

with 3 starting poses and 4 objects (*toilet, sofa, TV, trash-can*) positioned to accommodate the robot’s lower height, ensuring that the objects can be visible from its lower viewpoint.

Human Evaluation To further demonstrate our policy’s generalization capability to unseen embodiments, we evaluate it as a navigation assistant with humans as new, unseen embodiments. We asked 5 participants to navigate



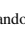




Model	Train Embodiment	Object	Human Participants					Average
			H1	H2	H3	H4	H5	
FLaRE [24]	Stretch RE-1		✓	✗	✗	✗	✗	40.0%
			✗	✗	✗	✗	✓	
RING-ZERO-SHOT	RING-Random		✓	✗	✗	✗	✓	73.3%
			✗	✓	✓	✓	✓	

Table 4. **Human Evaluation.** Five individuals navigate to 3 different objects (, , ) following the policy’s output actions on their phones in a kitchen area (example trajectories in Fig. 5). RING-ZERO-SHOT shows much better generalization to human embodiment than the FLaRE baseline trained on Stretch RE-1.

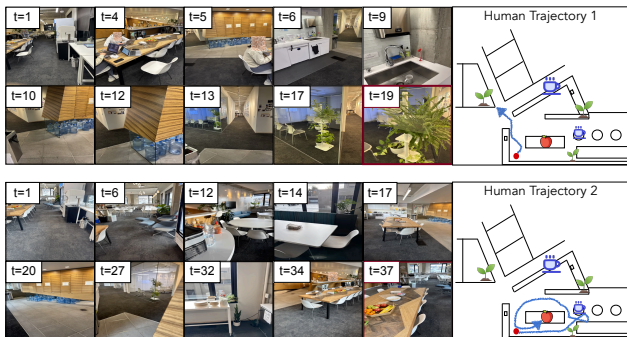


Figure 5. **Human Trajectories.** Two sample trajectories from two individuals navigating to a houseplant and an apple using RING.

in a real-world kitchen area, following the policy’s output actions on their phones. Each individual has unique characteristics, including step size, height, rotation angles, and camera-holding posture. Each person navigates to three different objects (Mug, Apple, Houseplant), resulting in a total of 15 trajectories. We compare RING with FLaRe [24], which was trained exclusively on the Stretch RE-1. Tab. 4 shows that RING consistently outperforms FLaRe across target objects and different participants. Fig. 5 shows two qualitative results achieved by RING (more details about human evaluation Appendix 6.2).

4.3. RING can efficiently adapt to an embodiment-specialized policy with minimal finetuning

Although RING is a universal policy that works zero-shot across a broad range of embodiments, there are often cases where an embodiment-specialized policy is needed to achieve the best performance. In this section, we demonstrate that RING can be easily adapted to a *robot-specialized policy* with minimal fine-tuning, resulting in better performance on the target embodiment.

Baselines. We use FLaRe [24] as a baseline. It has shown successful adaptation to new tasks and embodiments. This baseline is pretrained on Stretch RE-1 and finetuned on each of the three embodiments using up to 20M RL steps.

Implementation Details. We finetune RING, pretrained on randomized embodiments, on each individual robot for up to 20M RL steps, while keeping all hyperparameters consistent with FLaRe to ensure a fair comparison. Following FLaRe, we repurpose two actions `RotateBase` ($\pm 6^\circ$) to `TiltCamera` ($\pm 30^\circ$) to allow camera movements for LoCoBot. Note that this movement is not allowed during the zero-shot evaluation.

Results. Fig. 7 shows that RING adapts efficiently to specific embodiments with minimal finetuning, leading to embodiment-specialized policies with even better performance. For LoCoBot and Unitree-A1, FLaRe’s performance remains lower than on Stretch RE-1, indicating that pretraining on one embodiment and finetuning across embodiments cannot achieve the best results. This highlights the need for a policy that can consistently adapt to any embodiment with lightweight finetuning.

4.4. RING has embodiment-adaptive behavior.

The behavior of optimal navigation policy, $\pi_\theta^*(a_t | o_t^e)$, should be strongly shaped by the agent’s body. For instance, an agent with a narrow FOV must explore more to effectively perceive its surroundings compared to an agent with a wider FOV. A smaller agent can navigate through narrow hallways or under furniture, and a larger agent may need to take more conservative paths. A question arises: does the policy show the same navigation behaviors across different embodiments, or does it adjust its strategy accordingly?

Our qualitative results confirm that the policy has an **embodiment-adaptive behavior**. In Fig. 6-A,B, both Stretch RE-1 and Unitree A1 start from the same pose behind the bed. The quadruped robot directly moves under the bed because of its lower height, while the Stretch RE-1 bypasses it. We observe that RING *implicitly* infers embodiment parameters from visual observations and transition dynamics, dynamically adjusting its navigation strategy accordingly. It does not have access to any privileged information about its current body.

Visual observation reveals parameters, such as camera specs and, in some cases, agent height. However, visual information alone can be insufficient, leading the agent to rely on collisions to infer body dimensions. In Fig. 6-C, the agent matches the Stretch RE-1’s height but has a camera positioned as low as the quadruped’s. Initially, it assumes a lower height and attempts to go under the bed, but after colliding, it adjusts to maneuver around the bed, similar to the Stretch RE-1. This embodiment-adaptive navigation strategy adjustment is an interesting emergent behavior that would not have been possible without training across the exhaustive space of embodiments at scale.

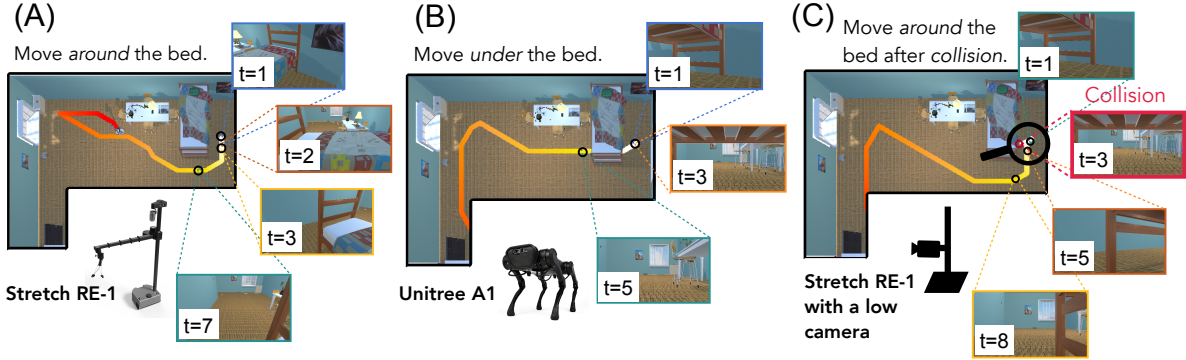


Figure 6. RING has **embodiment-adaptive** behavior, adjusting its navigation strategy based on the embodiment. The quadruped robot (B), due to its lower height, walks under the bed, while the taller Stretch-RE1 robot (A) navigates around it. In (C), an agent with the same height as Stretch-RE1 but a lower camera position initially attempts to move under the bed, assuming a shorter height. After colliding, it adapts its strategy and navigates around the bed, similar to Stretch-RE1.

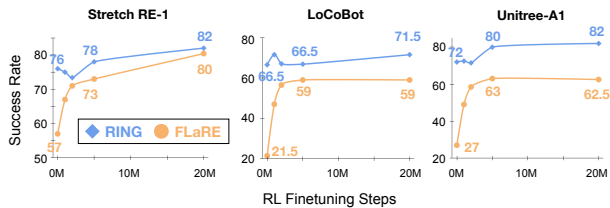


Figure 7. **Embodiment-Specialized Adaptation.** RING, pre-trained on randomized embodiments, shows efficient adaptation to robot-specialized policies with minimal fine-tuning. Baseline performance on LoCoBot and Unitree-A1 remains lower as they are fine-tuned on a different embodiment than the one used in pretraining. In contrast, RING policy achieves consistent performance across all 3 embodiments, highlighting its capability for robot-specialized adaptation.

4.5. Ablation Studies

A More Powerful Pretrained Visual Encoder. The default vision encoder used in our policies is the pretrained SIGLIP-ViT-B/16. In this section, we examine the impact of using a more powerful visual encoder on RING’s performance. We train RING-LARGE using OpenAI’s ViT-L/14 336PX CLIP model [38]. Table 5 compares the results, showing that a stronger visual encoder significantly improves zero-shot performance across all four embodiments (approximately 9% improvement on average). A larger visual encoder is particularly beneficial in our policy, as the visual observations are highly varied due to randomized camera parameters. To ensure fair comparison with the baselines and because ViT-L/14 is more computationally demanding, we chose to use the ViT-B/16 encoder for our main experiments. We will release the training code for the community for those interested in training with the larger visual encoder.

Model	Visual Encoder	Benchmark Embodiment			
		Stretch	Stretch _(Nav)	LoCoBot	Unitree A1
RING	SIGLIP-ViT-B/16	76.0	74.0	66.5	72.0
RING-LARGE	ViT-L/14 336PX CLIP	83.8	77.7	75.3	79.9

Table 5. **A Stronger Visual Encoder.** Using a more powerful vision encoder significantly improves the zero-shot performance across all embodiments.

Model	Collision Penalty	Metrics				
		Success ↑	SEL ↑	SC ↑	CR ↓	Safe Episode ↑
RING	✗	67.62	56.24	42.53	7.77	46.90
	✓	66.33	56.87	49.05	4.03	60.57

Table 6. **Collision Penalty.** Adding a small collision penalty (0.1) to the reward function results in 50% less collision, forcing the policy to take more conservative paths.

Include collision penalty to take safer routes. As our agents have randomized body dimensions and are not explicitly informed about their embodiment, they may occasionally collide before understanding their correct body size. In this section, we demonstrate that adding a small collision penalty of 0.1 to the reward function can reduce collisions rate by 50% (lowering the collision rate *CR* from 7% to 4%). The resulting policy is more conservative, regardless of embodiment size.

To quantify these results, we created a custom benchmark similar to CHORES-S [17], consisting of 2,000 random embodiments across 2,000 scenes. We evaluate 2 different versions of our policy on this benchmark, comparing metrics such as *Success Rate*, *Success Weighted by Collision (SC)*, *Collision Rate (CR)*, and *Safe Episode (percentage of episodes without any collisions)*. As shown in Table 6, adding the collision penalty reduces the collision rate (CR) (7.77% → 4.03%) as well as increases the percentage of trajectories without collisions (46.90% → 60.57%).

5. Conclusion

In this paper, we introduce RING (**R**obotic **I**ndoor **N**avigation **G**eneralist), an embodiment-agnostic policy, trained solely in simulation with diverse randomly initialized embodiments at scale (1M embodiments). RING displays zero-shot generalization capability to various unseen embodiments, maintaining consistent performance across all. Our experimental results demonstrate that RING achieves state-of-the-art results on novel embodiments, including in some cases improving over embodiment-specific policies. It can be directly deployed to the real-world despite being solely trained in simulation. Finally, RING is able to dynamically adjust its behavior based on its embodiment and interactions with the environment.

References

- [1] Michael Ahn, Anthony Brohan, Noah Brown, Yevgen Chebotar, Omar Cortes, Byron David, Chelsea Finn, Chuyuan Fu, Keerthana Gopalakrishnan, Karol Hausman, et al. Do as i can, not as i say: Grounding language in robotic affordances. *CoRL*, 2022. 3
- [2] Dhruv Batra, Aaron Gokaslan, Aniruddha Kembhavi, Oleksandr Maksymets, Roozbeh Mottaghi, Manolis Savva, Alexander Toshev, and Erik Wijnmans. ObjectNav revisited: On evaluation of embodied agents navigating to objects. *CoRR*, abs/2006.13171, 2020. 3
- [3] Homanga Bharadhwaj, Roozbeh Mottaghi, Abhinav Gupta, and Shubham Tulsiani. Track2act: Predicting point tracks from internet videos enables generalizable robot manipulation. In *ECCV*, 2024. 2
- [4] Nico Bohlinger, Grzegorz Czechmanowski, Maciej Piotr Krupka, Piotr Kicki, Krzysztof Walas, Jan Peters, and Davide Tateo. One policy to run them all: Towards an end-to-end learning approach to multi-embodiment locomotion. In *CoRL*, 2024. 3
- [5] Anthony Brohan, Noah Brown, Justice Carbajal, Yevgen Chebotar, Xi Chen, Krzysztof Choromanski, Tianli Ding, Danny Driess, Avinava Dubey, Chelsea Finn, Pete Florence, Chuyuan Fu, Montse Gonzalez Arenas, Keerthana Gopalakrishnan, Kehang Han, Karol Hausman, Alexander Herzog, Jasmine Hsu, Brian Ichter, Alex Irpan, Nikhil J. Joshi, Ryan Julian, Dmitry Kalashnikov, Yuheng Kuang, Isabel Leal, Lisa Lee, Tsang-Wei Edward Lee, Sergey Levine, Yao Lu, Henryk Michalewski, Igor Mordatch, Karl Pertsch, Kanishka Rao, Krista Reymann, Michael S. Ryoo, Grecia Salazar, Pannag Sanketi, Pierre Sermanet, Jaspier Singh, Anikait Singh, Radu Soricut, Huong T. Tran, Vincent Vanhoucke, Quan Vuong, Ayzaan Wahid, Stefan Welker, Paul Wohlhart, Jialin Wu, Fei Xia, Ted Xiao, Peng Xu, Sichun Xu, Tianhe Yu, and Brianna Zitkovich. RT-2: vision-language-action models transfer web knowledge to robotic control. *CoRR*, abs/2307.15818, 2023. 2
- [6] Devendra Singh Chaplot, Dhiraj Gandhi, Saurabh Gupta, Abhinav Gupta, and Ruslan Salakhutdinov. Learning to explore using active neural slam. *ICLR*, 2020. 3
- [7] Lawrence Yunliang Chen, Chenfeng Xu, Karthik Dharmarajan, Zubair Irshad, Richard Cheng, Kurt Keutzer, Masayoshi Tomizuka, Quan Vuong, and Ken Goldberg. Rovi-aug: Robot and viewpoint augmentation for cross-embodiment robot learning. In *CoRL*, 2024. 2
- [8] Xiaoyu Chen, Jiachen Hu, Chi Jin, Lihong Li, and Liwei Wang. Understanding Domain Randomization for Sim-to-real Transfer. In *The Tenth International Conference on Learning Representations, ICLR 2022, Virtual Event, April 25-29, 2022*. OpenReview.net, 2022. 3
- [9] Open X-Embodiment Collaboration, Abby O’Neill, Abdul Rehman, Abhinav Gupta, Abhiram Maddukuri, Abhishek Gupta, Abhishek Padalkar, Abraham Lee, Acorn Pooley, Agrim Gupta, Ajay Mandelkar, Ajinkya Jain, Albert Tung, Alex Bewley, Alex Herzog, Alex Irpan, Alexander Khazatsky, Anant Rai, Anchit Gupta, Andrew Wang, Andrey Kolobov, Anikait Singh, Animesh Garg, Aniruddha Kembhavi, Annie Xie, Anthony Brohan, Antonin Raffin, Archit Sharma, Arefeh Yavary, Arhan Jain, Ashwin Balakrishna, Ayzaan Wahid, Ben Burgess-Limerick, Beomjoon Kim, Bernhard Schölkopf, Blake Wulfe, Brian Ichter, Cewu Lu, Charles Xu, Charlotte Le, Chelsea Finn, Chen Wang, Chenfeng Xu, Cheng Chi, Chenguang Huang, Christine Chan, Christopher Agia, Chuer Pan, Chuyuan Fu, Coline Devin, Danfei Xu, Daniel Morton, Danny Driess, Daphne Chen, Deepak Pathak, Dhruv Shah, Dieter Büchler, Dinesh Jayaraman, Dmitry Kalashnikov, Dorsa Sadigh, Edward Johns, Ethan Foster, Fangchen Liu, Federico Ceola, Fei Xia, Feiyu Zhao, Felipe Vieira Frujeri, Freek Stulp, Gaoyue Zhou, Gaurav S. Sukhatme, Gautam Salhotra, Ge Yan, Gilbert Feng, Giulio Schiavi, Glen Berseth, Gregory Kahn, Guangwen Yang, Guanzhi Wang, Hao Su, Hao-Shu Fang, Haochen Shi, Henghui Bao, Heni Ben Amor, Henrik I Christensen, Hiroki Furuta, Homanga Bharadhwaj, Homer Walke, Hongjie Fang, Huy Ha, Igor Mordatch, Ilija Radosavovic, Isabel Leal, Jacky Liang, Jad Abou-Chakra, Jachyung Kim, Jaimyn Drake, Jan Peters, Jan Schneider, Jasmine Hsu, Jay Vakil, Jeannette Bohg, Jeffrey Bingham, Jeffrey Wu, Jensen Gao, Jiaheng Hu, Jiajun Wu, Jialin Wu, Jiankai Sun, Jianlan Luo, Jiayuan Gu, Jie Tan, Jihoon Oh, Jimmy Wu, Jingpei Lu, Jingyun Yang, Jitendra Malik, João Silvério, Joey Hejna, Jonathan Booher, Jonathan Tompson, Jonathan Yang, Jordi Salvador, Joseph J. Lim, Junhyek Han, Kaiyuan Wang, Kanishka Rao, Karl Pertsch, Karol Hausman, Keegan Go, Keerthana Gopalakrishnan, Ken Goldberg, Kendra Byrne, Kenneth Oslund, Kento Kawaharazuka, Kevin Black, Kevin Lin, Kevin Zhang, Kiana Ehsani, Kiran Lekkala, Kirsty Ellis, Krishan Rana, Krishnan Srinivasan, Kuan Fang, Kunal Pratap Singh, Kuo-Hao Zeng, Kyle Hatch, Kyle Hsu, Laurent Itti, Lawrence Yunliang Chen, Lerrel Pinto, Li Fei-Fei, Liam Tan, Linxi ”Jim” Fan, Lionel Ott, Lisa Lee, Luca Weihs, Magnum Chen, Marion Lepert, Marius Memmel, Masayoshi Tomizuka, Masha Itkina, Mateo Guaman Castro, Max Spero, Maximilian Du, Michael Ahn, Michael C. Yip, Mingtong Zhang, Mingyu Ding, Minh Heo, Mohan Kumar Srirama, Mohit Sharma, Moo Jin Kim, Naoaki Kanazawa, Nicklas Hansen, Nicolas Heess, Nikhil J Joshi, Niko Suennderhauf, Ning Liu, Norman Di Palo, Nur Muhammad Mahi

- Shafiqullah, Oier Mees, Oliver Kroemer, Osbert Bastani, Pannag R Sanketi, Patrick "Tree" Miller, Patrick Yin, Paul Wohlhart, Peng Xu, Peter David Fagan, Peter Mitrano, Pierre Sermanet, Pieter Abbeel, Priya Sundareshan, Qiuyu Chen, Quan Vuong, Rafael Rafailov, Ran Tian, Ria Doshi, Roberto Mart'in-Mart'in, Rohan Baijal, Rosario Scalise, Rose Hendrix, Roy Lin, Runjia Qian, Ruohan Zhang, Russell Mendonca, Rutav Shah, Ryan Hoque, Ryan Julian, Samuel Bustamante, Sean Kirmani, Sergey Levine, Shan Lin, Sherry Moore, Shikhar Bahl, Shivin Dass, Shubham Sonawani, Shubham Tulsiani, Shuran Song, Sichun Xu, Siddhant Hal-dar, Siddharth Karamcheti, Simeon Adebola, Simon Guist, Soroush Nasiriany, Stefan Schaal, Stefan Welker, Stephen Tian, Subramanian Ramamoorthy, Sudeep Dasari, Suneel Belkhale, Sungjae Park, Suraj Nair, Suvir Mirchandani, Takayuki Osa, Tanmay Gupta, Tatsuya Harada, Tatsuya Mat-sushima, Ted Xiao, Thomas Kollar, Tianhe Yu, Tianli Ding, Todor Davchev, Tony Z. Zhao, Travis Armstrong, Trevor Darrell, Trinity Chung, Vidhi Jain, Vikash Kumar, Vincent Vanhoucke, Wei Zhan, Wenxuan Zhou, Wolfram Burgard, Xi Chen, Xiangyu Chen, Xiaolong Wang, Xinghao Zhu, Xinyang Geng, Xiyuan Liu, Xu Liangwei, Xuanlin Li, Yan-song Pang, Yao Lu, Yecheng Jason Ma, Yejin Kim, Yevgen Chebotar, Yifan Zhou, Yifeng Zhu, Yilin Wu, Ying Xu, Yixuan Wang, Yonatan Bisk, Yongqiang Dou, Yoonyoung Cho, Youngwoon Lee, Yuchen Cui, Yue Cao, Yueh-Hua Wu, Yujin Tang, Yuke Zhu, Yunchu Zhang, Yunfan Jiang, Yunshuang Li, Yunzhu Li, Yusuke Iwasawa, Yutaka Matsuo, Zehan Ma, Zhuo Xu, Zichen Jeff Cui, Zichen Zhang, Zipeng Fu, and Zipeng Lin. Open X-Embodiment: Robotic learning datasets and RT-X models. In *ICRA*, 2024. 2
- [10] Matt Deitke, Rose Hendrix, Luca Weihs, Ali Farhadi, Kiana Ehsani, and Aniruddha Kembhavi. Phone2Proc: Bringing robust robots into our chaotic world, 2022. 6, 4
- [11] Matt Deitke, Dustin Schwenk, Jordi Salvador, Luca Weihs, Oscar Michel, Eli VanderBilt, Ludwig Schmidt, Kiana Ehsani, Aniruddha Kembhavi, and Ali Farhadi. Objaverse: A Universe of Annotated 3D Objects. *2023 IEEE/CVF Conference on Computer Vision and Pattern Recognition (CVPR)*, pages 13142–13153, 2022. 2, 3
- [12] Matt Deitke, Eli VanderBilt, Alvaro Herrasti, Luca Weihs, Kiana Ehsani, Jordi Salvador, Winson Han, Eric Kolve, Aniruddha Kembhavi, and Roozbeh Mottaghi. ProcTHOR: Large-scale embodied AI using procedural generation. In *NeurIPS*, 2022. 2, 5, 6
- [13] Ria Doshi, Homer Walke, Oier Mees, Sudeep Dasari, and Sergey Levine. Scaling cross-embodied learning: One policy for manipulation, navigation, locomotion and aviation. *arXiv preprint arXiv:2408.11812*, 2024. 2
- [14] Jiafei Duan, Wentao Yuan, Wilbert Pumacay, Yi Ru Wang, Kiana Ehsani, Dieter Fox, and Ranjay Krishna. Manipulate anything: Automating real-world robots using vision-language models. *arXiv preprint arXiv:2406.18915*, 2024. 2
- [15] Ainaz Eftekhari, Kuo-Hao Zeng, Jiafei Duan, Ali Farhadi, Ani Kembhavi, and Ranjay Krishna. Selective visual representations improve convergence and generalization for embodied ai. In *ICLR*, 2023. 3, 6
- [16] Kiana Ehsani, Tanmay Gupta, Rose Hendrix, Jordi Salvador, Luca Weihs, Kuo-Hao Zeng, Kunal Pratap Singh, Yejin Kim, Winson Han, Alvaro Herrasti, et al. Imitating shortest paths in simulation enables effective navigation and manipulation in the real world. In *CVPR*, 2024. 5, 6, 4
- [17] Kiana Ehsani, Tanmay Gupta, Rose Hendrix, Jordi Salvador, Luca Weihs, Kuo-Hao Zeng, Kunal Pratap Singh, Yejin Kim, Winson Han, Alvaro Herrasti, et al. Spoc: Imitating shortest paths in simulation enables effective navigation and manipulation in the real world, pages 16238–16250, 2024. 2, 3, 5, 6, 8, 1, 4
- [18] Allen Institute for AI. ObjathOR: Python package for importing and loading external assets into ai2thor. <https://github.com/allenai/objathor>, 2024. 5
- [19] Huy Ha, Yihuai Gao, Zipeng Fu, Jie Tan, and Shuran Song. Umi on legs: Making manipulation policies mobile with manipulation-centric whole-body controllers. In *CoRL*, 2024. 2
- [20] Aric A. Hagberg, Daniel A. Schult, Pieter Swart, and JM Hagberg. Exploring Network Structure, Dynamics, and Function using NetworkX. *Proceedings of the Python in Science Conference*, 2008. 2
- [21] Sudarshan Harithas and Srinath Sridhar. Motionplot: A multi-embodied motion generation model. *arXiv preprint arXiv:2410.16623*, 2024. 2
- [22] Peter E. Hart, Nils J. Nilsson, and Bertram Raphael. A Formal Basis for the Heuristic Determination of Minimum Cost Paths. *IEEE Trans. Syst. Sci. Cybern.*, 4:100–107, 1968. 2
- [23] Joey Hejna, Chethan Bhateja, Yichen Jian, Karl Pertsch, and Dorsa Sadigh. Re-mix: Optimizing data mixtures for large scale imitation learning. In *CoRL*, 2024. 2
- [24] Jiaheng Hu, Rose Hendrix, Ali Farhadi, Aniruddha Kembhavi, Roberto Martin-Martin, Peter Stone, Kuo-Hao Zeng, and Kiana Ehsani. Flare: Achieving masterful and adaptive robot policies with large-scale reinforcement learning fine-tuning. *arXiv preprint arXiv:2409.16578*, 2024. 2, 3, 5, 6, 7, 4
- [25] Kushal Kedia, Prithwish Dan, and Sanjiban Choudhury. One-shot imitation under mismatched execution. *arXiv preprint arXiv:2409.06615*, 2024. 2
- [26] Mukul Khanna, Ram Ramrakhyia, Gunjan Chhablani, Sriram Yenamandra, Theophile Gervet, Matthew Chang, Zsolt Kira, Devendra Singh Chaplot, Dhruv Batra, and Roozbeh Mottaghi. Goat-bench: A benchmark for multi-modal lifelong navigation. In *CVPR*, 2024. 3
- [27] Alexander Khazatsky, Karl Pertsch, Suraj Nair, Ashwin Balakrishna, Sudeep Dasari, Siddharth Karamcheti, Soroush Nasiriany, Mohan Kumar Srirama, Lawrence Yunliang Chen, Kirsty Ellis, et al. DROID: A large-scale in-the-wild robot manipulation dataset. In *arXiv preprint arXiv:2403.12945*, 2024. 2
- [28] Moo Jin Kim, Karl Pertsch, Siddharth Karamcheti, Ted Xiao, Ashwin Balakrishna, Suraj Nair, Rafael Rafailov, Ethan Foster, Grace Lam, Pannag Sanketi, et al. Openvla: An open-source vision-language-action model. In *CoRL*, 2024. 2
- [29] Eric Kolve, Roozbeh Mottaghi, Winson Han, Eli VanderBilt, Luca Weihs, Alvaro Herrasti, Matt Deitke, Kiana Ehsani,

- Daniel Gordon, Yuke Zhu, Aniruddha Kembhavi, Abhinav Kumar Gupta, and Ali Farhadi. AI2-THOR: An Interactive 3D Environment for Visual AI. *ArXiv*, abs/1712.05474, 2017. 4, 5
- [30] Antonio Loquercio, Ana I Maqueda, Carlos R Del-Blanco, and Davide Scaramuzza. Dronet: Learning to fly by driving. In *RA-L*, 2018. 2
- [31] Arjun Majumdar, Gunjan Aggarwal, Bhavika Devnani, Judy Hoffman, and Dhruv Batra. ZSON: zero-shot object-goal navigation using multimodal goal embeddings. In *NeurIPS*, 2022. 3
- [32] Soroush Nasiriany, Fei Xia, Wenhao Yu, Ted Xiao, Jacky Liang, Ishita Dasgupta, Annie Xie, Danny Driess, Ayzaan Wahid, Zhuo Xu, et al. Pivot: Iterative visual prompting elicits actionable knowledge for vlms. *ICML*, 2024. 3
- [33] Octo Model Team, Dibya Ghosh, Homer Walke, Karl Pertsch, Kevin Black, Oier Mees, Sudeep Dasari, Joey Hejna, Charles Xu, Jianlan Luo, Tobias Kreiman, You Liang Tan, Pannag Sanketi, Quan Vuong, Ted Xiao, Dorsa Sadigh, Chelsea Finn, and Sergey Levine. Octo: An open-source generalist robot policy. In *RSS*, 2024. 2
- [34] Abby O’Neill, Abdul Rehman, Abhinav Gupta, Abhiram Maddukuri, Abhishek Gupta, Abhishek Padalkar, Abraham Lee, Acorn Pooley, Agrim Gupta, Ajay Mandlekar, et al. Open x-embodiment: Robotic learning datasets and rt-x models. *arXiv preprint arXiv:2310.08864*, 2023. 2
- [35] Maxime Oquab, Timothée Darcet, Theo Moutakanni, Huy V. Vo, Marc Szafranec, Vasil Khalidov, Pierre Fernandez, Daniel Haziza, Francisco Massa, Alaaeldin El-Nouby, Russell Howes, Po-Yao Huang, Hu Xu, Vasu Sharma, Shangwen Li, Wojciech Galuba, Mike Rabbat, Mido Assran, Nicolas Ballas, Gabriel Synnaeve, Ishan Misra, Herve Jegou, Julien Mairal, Patrick Labatut, Armand Joulin, and Piotr Bojanowski. DINOv2: Learning robust visual features without supervision, 2023. 3
- [36] Austin Patel and Shuran Song. GET-Zero: Graph Embodiment Transformer for Zero-shot Embodiment Generalization. *CoRR*, abs/2407.15002, 2024. 3
- [37] Xavier Puig, Eric Undersander, Andrew Szot, Mikael Dal-laire Cote, Tsung-Yen Yang, Ruslan Partsey, Ruta Desai, Alexander William Clegg, Michal Hlavac, So Yeon Min, Vladimir Vondrus, Théophile Gervet, Vincent-Pierre Berges, John M. Turner, Oleksandr Maksymets, Zsolt Kira, Mrinal Kalakrishnan, Jitendra Malik, Devendra Singh Chaplot, Unnat Jain, Dhruv Batra, Akshara Rai, and Roozbeh Mottaghi. Habitat 3.0: A Co-Habitat for Humans, Avatars and Robots. *CoRR*, abs/2310.13724, 2023. 3
- [38] Alec Radford, Jong Wook Kim, Chris Hallacy, Aditya Ramesh, Gabriel Goh, Sandhini Agarwal, Girish Sastry, Amanda Askell, Pamela Mishkin, Jack Clark, et al. Learning transferable visual models from natural language supervision. In *International conference on machine learning*, pages 8748–8763. PMLR, 2021. 8
- [39] Ilija Radosavovic, Tete Xiao, Bike Zhang, Trevor Darrell, Jitendra Malik, and Koushil Sreenath. Real-world humanoid locomotion with reinforcement learning. *Science Robotics*, 2024. 3
- [40] Ram Ramrakhya, Eric Undersander, Dhruv Batra, and Abhishek Das. Habitat-web: Learning embodied object-search strategies from human demonstrations at scale. In *IEEE/CVF Conference on Computer Vision and Pattern Recognition, CVPR 2022, New Orleans, LA, USA, June 18-24, 2022*, pages 5163–5173. IEEE, 2022. 3
- [41] Milad Shafiee, Guillaume Bellegarda, and Auke Ijspeert. Manyquadrupeds: Learning a single locomotion policy for diverse quadruped robots. In *ICRA*, 2024. 3
- [42] Dhruv Shah, Ajay Sridhar, Noriaki Hirose, and Sergey Levine. Gnm: A general navigation model to drive any robot. In *2023 IEEE International Conference on Robotics and Automation (ICRA)*, pages 7226–7233. IEEE, 2023. 2, 3
- [43] Dhruv Shah, Ajay Sridhar, Nitish Dashora, Kyle Stachowicz, Kevin Black, Noriaki Hirose, and Sergey Levine. Vint: A foundation model for visual navigation. *arXiv preprint arXiv:2306.14846*, 2023. 2, 3
- [44] Ajay Sridhar, Dhruv Shah, Catherine Glossop, and Sergey Levine. Nomad: Goal masked diffusion policies for navigation and exploration. In *ICRA*, 2023. 3
- [45] Octo Model Team, Dibya Ghosh, Homer Walke, Karl Pertsch, Kevin Black, Oier Mees, Sudeep Dasari, Joey Hejna, Tobias Kreiman, Charles Xu, et al. Octo: An open-source generalist robot policy. *arXiv preprint arXiv:2405.12213*, 2024. 2
- [46] Laurens Van der Maaten and Geoffrey Hinton. Visualizing data using t-sne. *Journal of machine learning research*, 9 (11), 2008. 2
- [47] Lirui Wang, Xinlei Chen, Jialiang Zhao, and Kaiming He. Scaling proprioceptive-visual learning with heterogeneous pre-trained transformers. In *NeurIPS*, 2024. 2
- [48] Saim Wani, Shivansh Patel, Unnat Jain, Angel X. Chang, and Manolis Savva. MultiON: Benchmarking Semantic Map Memory using Multi-Object Navigation. In *Advances in Neural Information Processing Systems 33: Annual Conference on Neural Information Processing Systems 2020, NeurIPS 2020, December 6-12, 2020, virtual*, 2020. 3
- [49] Luca Weihs, Jordi Salvador, Klemen Kotar, Unnat Jain, Kuo-Hao Zeng, Roozbeh Mottaghi, and Aniruddha Kembhavi. AllenAct: A framework for embodied ai research. *arXiv preprint arXiv:2008.12760*, 2020. 5
- [50] Erik Wijmans, Abhishek Kadian, Ari Morcos, Stefan Lee, Irfan Essa, Devi Parikh, Manolis Savva, and Dhruv Batra. DD-PPO: learning near-perfect pointgoal navigators from 2.5 billion frames. In *8th International Conference on Learning Representations, ICLR 2020, Addis Ababa, Ethiopia, April 26-30, 2020*. OpenReview.net, 2020. 3
- [51] Wenli Xiao, Haoru Xue, Tony Tao, Dvij Kalaria, John M Dolan, and Guanya Shi. Anycar to anywhere: Learning universal dynamics model for agile and adaptive mobility. *arXiv preprint arXiv:2409.15783*, 2024. 3
- [52] Mengda Xu, Zhenjia Xu, Cheng Chi, Manuela Veloso, and Shuran Song. Xskill: Cross embodiment skill discovery. In *CoRL*, 2023. 2
- [53] Mengda Xu, Zhenjia Xu, Yinghao Xu, Cheng Chi, Gordon Wetzstein, Manuela Veloso, and Shuran Song. Flow as the cross-domain manipulation interface. In *CoRL*, 2024. 2

- [54] Zhuo Xu, Hao-Tien Lewis Chiang, Zipeng Fu, Mithun George Jacob, Tingnan Zhang, Tsang-Wei Edward Lee, Wenhao Yu, Connor Schenck, David Rendleman, Dhruv Shah, et al. Mobility v1a: Multimodal instruction navigation with long-context vlms and topological graphs. In *CoRL*. 3
- [55] Brian Yamauchi. A frontier-based approach for autonomous exploration. In *Proceedings 1997 IEEE International Symposium on Computational Intelligence in Robotics and Automation CIRA'97: Towards New Computational Principles for Robotics and Automation*, pages 146–151. IEEE, 1997. 3
- [56] Jonathan Yang, Catherine Glossop, Arjun Bhorkar, Dhruv Shah, Quan Vuong, Chelsea Finn, Dorsa Sadigh, and Sergey Levine. Pushing the limits of cross-embodiment learning for manipulation and navigation. In *arXiv preprint arXiv:2402.19432*, 2024. 2
- [57] Joel Ye, Dhruv Batra, Abhishek Das, and Erik Wijmans. Auxiliary tasks and exploration enable objectnav. *CoRR*, abs/2104.04112, 2021. 3
- [58] Naoki Yokoyama, Ram Ramrakhya, Abhishek Das, Dhruv Batra, and Sehoon Ha. Hm3d-ovon: A dataset and benchmark for open-vocabulary object goal navigation. *IROS*, 2024. 3
- [59] Wentao Yuan, Jiafei Duan, Valts Blukis, Wilbert Pumacay, Ranjay Krishna, Adithyavairavan Murali, Arsalan Mousavian, and Dieter Fox. Robopoint: A vision-language model for spatial affordance prediction for robotics. *arXiv preprint arXiv:2406.10721*, 2024. 3
- [60] Kevin Zakka, Andy Zeng, Pete Florence, Jonathan Tompson, Jeannette Bohg, and Debidatta Dwibedi. Xirl: Cross-embodiment inverse reinforcement learning. In *CoRL*, 2022. 2
- [61] Kuo-Hao Zeng, Luca Weihs, Ali Farhadi, and Roozbeh Mottaghi. Pushing it out of the way: Interactive visual navigation. In *Proceedings of the IEEE/CVF Conference on Computer Vision and Pattern Recognition*, 2021. 3
- [62] Kuo-Hao Zeng, Zichen Zhang, Kiana Ehsani, Rose Hendrix, Jordi Salvador, Alvaro Herrasti, Ross Girshick, Aniruddha Kembhavi, and Luca Weihs. Poliformer: Scaling on-policy rl with transformers results in masterful navigators. In *CoRL*, 2024. 2, 3, 4, 5, 6
- [63] Xiaohua Zhai, Basil Mustafa, Alexander Kolesnikov, and Lucas Beyer. Sigmoid loss for language image pre-training. *ICCV*, abs/2303.15343, 2023. 3

The One RING : a Robotic Indoor Navigation Generalist

Supplementary Material

The following items are provided in the Appendix:

- Details about the real-world evaluation robot platforms and human evaluation setup (App. 6),
- Data collection for randomized embodiments using expert planners in simulation (App. 7),
- Full experimental setup (App. 8),
- Model architecture details (App. 9),
- A visualization of the random embodiments in our training set, along with the 5 nearest neighbors to each of the real robots (Stretch-RE1, LoCoBot, Unitree A1) (App. 10),
- Out-of-distribution generalization for different embodiment parameters (App. 11), and
- Limitations (conditioning on explicit embodiment parameters) (App. 12).

On our website (one-ring-policy.allen.ai), we have

- Real-world qualitative videos of evaluating RING zero-shot on four different robot platforms, including Stretch RE-1 with our camera setup, Stretch RE-1 with factory camera configuration, LoCoBot, and Unitree GO1,
- Qualitative videos for human evaluation, using RING as navigation assistant,
- Videos showing our dataset of trajectories collected from random embodiments in simulation.

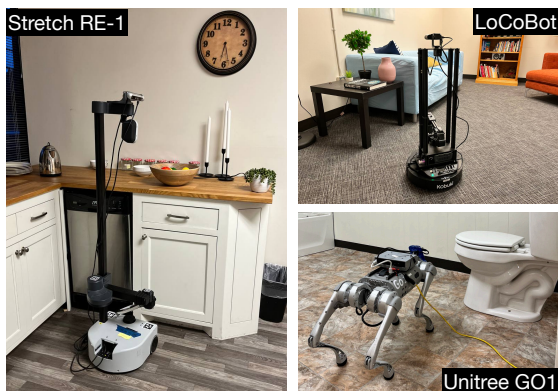


Figure 8. **Robot platforms.** We use 3 different platforms, including Stretch RE-1, LoCoBot, and Unitree GO1 for our real-world evaluations.

6. Real Robot Platforms and Human Evaluation Setup.

6.1. Stretch RE-1, LoCoBot, Unitree GO1

We use Stretch RE-1, LoCoBot, and Unitree GO1 as our robot platforms for real-world evaluations, shown in Fig. 8. For Stretch RE-1, we evaluate two different sensor configurations: the factory configuration and the configuration suggested by SPOC [17]. We summarize the main differences in these platform in Tab. 7. For robot movements, we either implement a Kalman filter or wrap around provided robot APIs to realize low-level controllers for a discrete action space $\{\text{MoveBase}(\pm 20\text{cm}), \text{RotateBase}(\pm 6^\circ, \pm 30^\circ), \text{Done}\}$ across all platforms. It is important to note that during the training stage, we do not use any embodiment configurations from these robots to generate imitation learning data or to initialize RL fine-tuning embodiments.



Figure 9. **Human Participants for Navigation Assistance.** Our five human participants have different height and different camera-holding poses, resulting in different sensory observations (details about human participants in Table 8).

6.2. Human Evaluations

Human participants. We asked five human participants to use RING as a navigation assistant and evaluated its performance across a range of different human embodiments. These variations stem from differences in camera-holding poses, participant heights, step sizes, and rotation angles. A summary of these variations across different participants can be found in Tab.8 and Fig.9. Due to these variations, each participant contributes a unique set of evaluation embodiments and sensor configurations.

Human evaluation details. We developed a simple iOS app, as shown in Fig. 10, that enables human participants to input the target object as text (e.g., Find a mug), capture an image using the iPhone’s back camera, and send

	Stretch RE-1	Stretch RE-1 (Factory)	LoCoBot	Unitree GO1
Body dimension (cm)	33 × 34 × 141	33 × 34 × 141	35 × 35 × 89	64.5 × 28 × 40
Camera model	2 × D455	D435	D435	D435
Camera vertical FoV (degrees)	59°	69°	42°	42°
Camera horizontal FoV (degrees)	90°	42°	68°	68°
Camera height (cm)	140	130	87	28
Camera pitch (degrees)	27°	30°	0°	0°

Table 7. **Details about evaluation robot platforms.** Our four robot platforms have varying dimensions and camera configurations, resulting in diverse evaluation embodiments.

	H1	H2	H3	H4	H5
Height	6'3"	5'10"	5'5"	6'1"	5'11"
Step size	0.25m	0.35m	0.4m	0.3m	0.3m
Rotation Degrees	30°	45°	45°	35°	30°

Table 8. **Details about human evaluators.** Our five human participants have varying heights, step size, and rotation degrees, resulting in different evaluation embodiments.

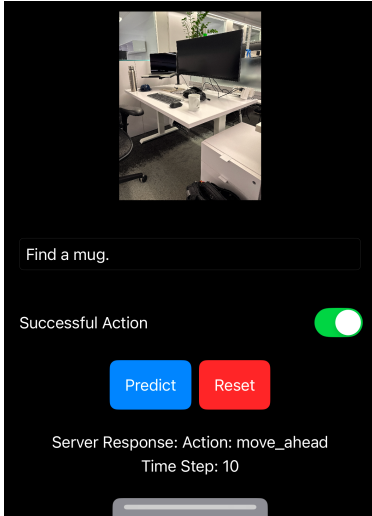


Figure 10. **iOS app for human evaluation.** We developed a simple iOS app that enables human participants to text goal, capture an image using iPhone’s back camera, send both to a remote server, and receive the predicted action from our RING policy.

both the text prompt and the captured image to a remote server. Upon receiving the prompt and image, the remote server processes them using our RING policy to predict action probabilities and samples an action. The predicted action is then sent back to the iPhone and displayed within the app. The prompted action space used is identical to that of our real-world robot.

The human participant navigates by following the suggested action at their own pace and rotation degree, as detailed in Tab. 8. After completing each action, they tap the

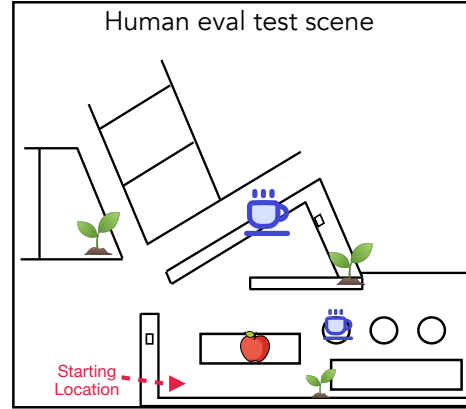


Figure 11. **Real-world test scene for human evaluation.** Three different target objects include (🍏 Apple, 🌱 Houseplant, ☕ Mug). The red arrow in the bottom left corner is the starting location.

Predict button again, prompting the app to capture a new image and send it to the server along with the text prompt. This process repeats until the Done action is returned or the 100th step is reached. An episode is considered successful if, before reaching 100 steps, the target object is visible in the latest image and within a 1 meter distance when RING calls Done.

The layout of the test scene is shown in Fig. 11, illustrating two locations for finding a Mug, three for a Houseplant, and one for an Apple. The participant always begins at the bottom-left corner of the scene.

7. Data Generation with Expert Planners

Expert planners introduced by [17] are not efficient and robust for random embodiments. As a result, we made major improvements to the planners to allow for better trajectories.

The major factor in this improvement is to consider *safety* of the policy (defined as the avoidance of approaching any obstacles along the way.) We use A* [20, 22] to generate safe navigation trajectories for training as follows: **1)** Extract reachable locations in a scene on a finely spaced grid, ensuring that the agent’s collider does not intersect

with any object’s collider. Thus, different embodiments yield different reachable locations according to their collider. **2)** Compute a clipped Euclidean distance to the nearest obstacle. Then, for each location, set the cost of visiting it as the inverse of the third power of the distance. **3)** Construct a grid-like graph where each reachable location is a node connected to its immediate neighbors. For each connection, assign a cost equal to the maximum cost of visiting either of the two connected nodes. **4)** Extract a minimum-cost path connecting the reachable positions in the graph nearest to the source and to the target via A*. **5)** Extract waypoints by skipping over points in the A* path as long as skipping them doesn’t increase the total path cost from the latest waypoint. **6)** The expert linearly interpolates between waypoints up to the precision reachable by the action space to generate each trajectory.

8. Additional Benchmark/Experiment Details

Action Space. Following on prior work with AI2-THOR, we discretize the action space for all agents in our training: $\{\text{MoveAhead}, \text{MoveBack}, \text{RotateRight}, \text{RotateLeft}, \text{RotateRightSmall}, \text{RotateLeftSmall}, \text{Done}\}$. Here, `MoveAhead` advances the robot by 0.2 meters, `MoveBack` moves the robot backward by 0.2 meters, `RotateRight`/`RotateRightSmall` rotates it clockwise by 30° / 6° around the yaw axis, and `RotateLeft`/`RotateLeftSmall` rotates it counterclockwise by 30° / 6° around the yaw axis, and `Done` indicates the agent has located the target, ending the episode. We evaluate RING zero-shot on all robots (Stretch-RE, LoCoBot, Unitree Go1) with the same action space using their low-level controllers. When finetuning for embodiment-specialized policies, we finetune for a slightly different action space for LoCoBot: $\{\text{MoveAhead}, \text{MoveBack}, \text{RotateRight}, \text{RotateLeft}, \text{LookUp}, \text{LookDown}, \text{Done}\}$. `LookUp` tilts the camera up by 30° around the roll axis and `LookDown` tilts the camera down by 30° around the roll axis. All baselines are trained and evaluated with the same action space for fair comparison.

Success Criteria. We follow the definition of Object Goal Navigation from [2], where an agent must explore its environment to locate and navigate to a specified object within a maximum of n steps. To indicate it has found the target, the agent must execute the `Done` action. Success is determined by the environment based on whether the agent is within a distance d of the target and if the target is visible in its view. If the agent exceeds n steps without executing the `Done` action, the episode is considered a failure. For simulation benchmarks, we follow CHORES-S [17] with $n = 600$ and $d = 2$. For real-world evaluations, we use $n = 300$ and $d = 1$.

Success weighted by collision (SC). Collision is one of the main challenges for a unified policy operating across diverse embodiments in visual navigation tasks. Previous works measure the collision rate ($\frac{\#collisions}{\#steps}$) to understand how often a policy collides with objects in a scene. However, this does not reflect the effectiveness of the policy at the task level. For example, in a successful episode, a single collision and multiple collisions should have different impacts on the performance measurement. As a results, inspired from Success Weighted by Episode Length (SEL), we propose Success Weighted by Collision (SC),

$$SC = \frac{1}{N} \sum_{i=1}^N S_i \frac{1}{1 + c_i}, \quad (2)$$

where S_i is a binary indicator of success for episode i , c_i is the number of collisions in episode i , and N is the number of evaluation episodes. In this metric, the policy is penalized most heavily for a single collision, with the penalization decreasing for each additional collision, as the penalty diminishes inversely with the number of collisions. Intuitively, > 0 collisions are much worse than 0, as a real robot may suffer damage from one bad collision, but the difference between 10 and 11 collisions is a more marginal difference.

Hyperparameters. We list the hyperparameters used in training and the architecture in Table 9.

Imitation Learning	
Batch Size	224
Context Length	100
Learning Rate	0.0002
RL Finetuning	
Total Rollouts	64
Learning Rate	0.0002
Mini Batch per Update	1
Update Repeats	4
Max Gradient Norm	0.5
Discount Value Factor γ	0.99
GAE λ	0.95
PPO Surrogate Objective Clipping	0.1
Value Loss Weight	0.5
Entropy Loss Weight	0.0
Steps for PPO Update	128
Model Architecture	
Transformer State Encoder Layers	3
Transformer State Encoder Hidden Dims	512
Transformer State Encoder Heads	8
Causal Transformer Deocder Layers	3
Causal Transformer Deocder Hidden Dims	512
Causal Transformer Deocder Heads	8

Table 9. Hyperparameters for training and model architecture.

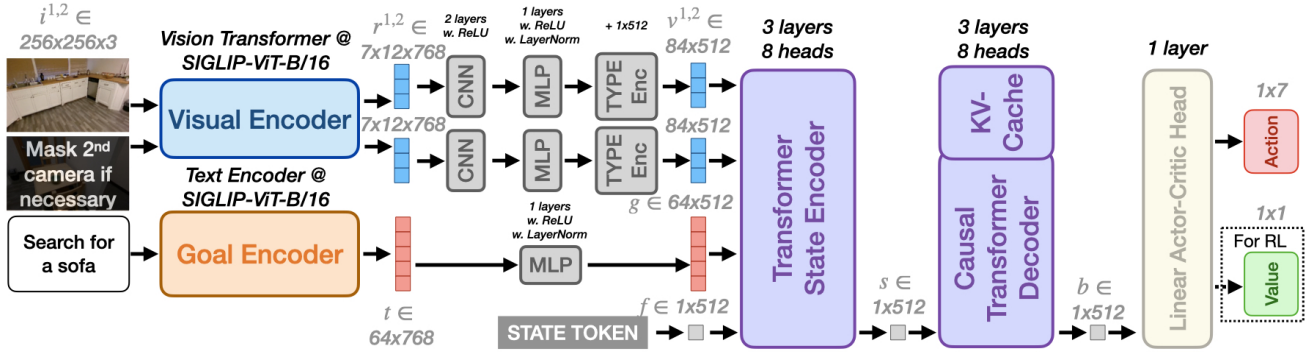


Figure 12. **RING architecture.** The notations in gray correspond to hidden feature vectors and the black text on top of each module indicates the hyperparameters for that module. RING accepts visual observations and a language instruction as inputs and predicts an action to execute. During RL finetuning, RING also predicts a value estimate. We mask the image from the 2^{nd} camera with all 0 for the embodiments with only one camera, such as LoCoBot and Unitree. More specifically, we use the Vision Transformer and the Text Encoder from SIGLIP-ViT-B/16 as our visual encoder and goal encoder. After encoding, we compress and project the visual representation r and text embedding t to v and g , respectively, with the desired dimension d . Next, the Transformer State Encoder encodes v , g , along with state token embedding f into a state feature vector s . The Causal Transformer Decoder further processes s , along with previous experiences stored in the KV-Cache, to produce the state belief b . Finally, the Linear Actor-Critic Head predicts action logits (and, during RL finetuning, a value estimate) from b .

8.1. Real-World Benchmarks

All robots are evaluated in a multi-room apartment shown in Fig. 4. Based on the embodiment, the benchmark has different starting locations and objects. Among our target object categories, `Apple` can be found in the Living room and Kitchen, `Bed` can only be found in the Bedroom, `Sofa` and `Television` can only be found in the Living room, `Vase` can be found in the Livingroom, Corridor, Office, and Kitchen, `Chair` can be found in the Office and Kitchen, `HousePlant` can be found in the Living room, Office, and Kitchen.

- **LoCoBot:** Following Phone2Proc [10], use the same five target object categories, including `Apple`, `Bed`, `Sofa`, `Television`, and `Vase`, and the three starting poses shown in 4.
- **Stretch RE-1:** We follow SPOC [16] to use the same six target object categories, including `Apple`, `Bed`, `Chair`, `HousePlant`, `Sofa`, and `Vase`, and the three starting poses, shown in Fig. 4. We consider 2 different camera configurations for Stretch: 1) off-the-shelf camera equipped on the Stretch RE-1 (D435 with a vertical field of view of 69° and resolution of 720×1280), 2) following [17], we use 2 Intel RealSense 455 fixed cameras, with a vertical field of view of 59° and resolution of 1280×720 . The cameras are mounted facing forward but pointing downward, with the horizon at an angle of 27° .
- **Unitree Go1:** We create a new evaluation set for Unitree Go1 with 3 starting poses (Fig. 4) and 4 objects (`toilet`, `sofa`, `TV`, `trashcan`) positioned

to accommodate the robot’s lower height, ensuring that the objects can be visible from its lower viewpoint.

9. Model Architecture Details

We will now detail RING’s architecture (see Fig. 12), which is inspired by previous works POLIFORMER [62] and FLARE [24].

Visual encoder. We use the Vision Transformer from the pretrained SIGLIP-ViT-B/16 as our visual encoder. Since the RGB images vary in dimensions across different embodiments, we include an additional preprocessing step before feeding them into the encoder. Specifically, we pad each RGB image to a square and then resize it to 256×256 . In addition, we mask the image from the 2^{nd} camera with zeros for the embodiments with only one camera. The visual backbone takes the RGB observation $i \in \mathbb{R}^{256 \times 256 \times 3}$ as input and produces a patch-wise representation $r \in \mathbb{R}^{\frac{256}{16} \times \frac{256}{16} \times h}$, where $h = 768$ is the hidden dimension of the visual representation. We reshape the visual representation into a $\ell \times h$ matrix, $\ell = 256 \cdot 256 / 16 \cdot 16$, and project the representation to produce $v \in \mathbb{R}^{\ell \times d}$, where $d = 512$ is the input dimension to the transformer state encoder. Note that since we have two RGB images from two cameras, we produce two visual representations $v^{1,2}$ at the end of this module. The vision encoder remains frozen through training.

Goal encoder. We follow the Text Transformer from the pretrained SIGLIP-ViT-B/16 to encode the given natural language instruction into goal embedding $t \in \mathbb{R}^{64 \times h}$, where $h = 768$ is the hidden dimension and this Text Transformer

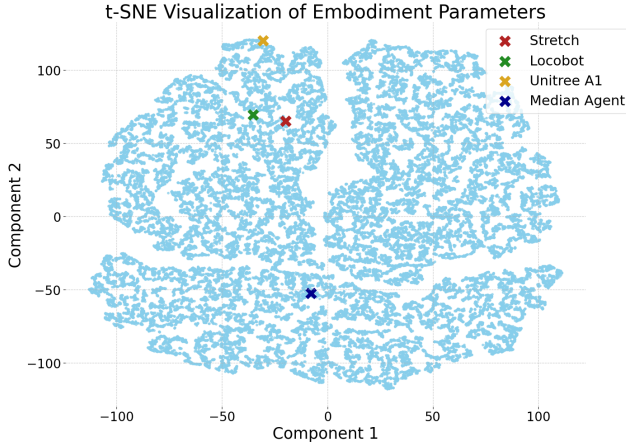


Figure 13. t-SNE visualization of the embodiment parameters $\mathbf{c}_e \in \mathbb{R}^{19}$ for 50k random agents. The three specific robots are also shown for visualization (they are not included in our training set).

returns 64 tokens after padding. Before passing the goal embedding to the transformer state encoder, we always project the embedding to the desired dimension $d = 512$, resulting in $g \in \mathbb{R}^{64 \times 512}$.

Transformer State Encoder. This module summarizes the state at each timestep as a vector $s \in \mathbb{R}^d$. The input to this encoder includes two visual representations $v^{1,2}$, the goal feature g , and an embedding f of a STATE token. These features are concatenated and fed to the non-causal transformer encoder. The output corresponding to the STATE token is the state feature vector $s \in \mathbb{R}^d$ which summarizes the state at each timestep. This feature vector is a goal-conditioned visual state representation.

Causal transformer decoder. We use a causal transformer decoder to perform explicit memory modeling over time. This can enable both long-horizon (*e.g.*, exhaustive exploration with backtracking) and short-horizon (*e.g.*, navigating around an object) planning. Concretely, the causal transformer decoder constructs its state belief b^t using the sequence of state features $\mathbf{s} = \{s^j\}_{j=0}^t$ within the same trajectories. To avoid recomputing the attention on the previous state features, we follow PoliFormer [62] to use KV-Cache to store the past **Key** and **Value** into two cache matrices in each attention layer. Therefore, we only perform feedforward computation for the most current state feature s^t .

Linear actor-critic head. With the latest state belief b^t , we simply use a linear actor-critic head to project it to predict action logits over the action space. For RL-finetuning, the linear actor-critic head also predicts a value estimate about the current state.

	Stretch RE-1	Nearest Neighbors				
		N1	N2	N3	N4	N5
Camera Position (x) (meters)	0	-0.06	0.11	0	-0.08	0.03
Camera Position (y) (meters)	1.44	1.13	0.67	0.24	0.72	0.32
Camera Position (z) (meters)	0.07	0.03	0.06	0.07	0.07	-0.03
Camera Pitch (degrees)	27	29	33	34	32	33
Camera Yaw (degrees)	0	0	0	0	0	0
Vertical FoV (degrees)	59	57	56	54	59	54
RGB Resolution (H)	224	224	224	224	224	224
RGB Resolution (Y)	396	394	394	396	396	398
Rotation Center (x) (meters)	0	0	0.09	-0.17	0	0.02
Rotation Center (z) (meters)	0.11	0.02	0.02	-0.08	0.04	-0.12
Collider Size (x) (meters)	0.34	0.23	0.28	0.49	0.33	0.24
Collider Size (y) (meters)	1.41	1.41	0.9	0.84	1.23	0.43
Collider Size (z) (meters)	0.33	0.27	0.41	0.29	0.44	0.38
distance	-	0.38	0.7	0.79	0.8	0.92

Table 10. Five Nearest Neighbor Embodiments for Stretch RE-1 in Training Data.

	Locobot	Nearest Neighbors				
		N1	N2	N3	N4	N5
Camera Position (x) (meters)	0	-0.09	0.12	0.03	-0.06	-0.1
Camera Position (y) (meters)	0.87	1.01	0.81	0.39	0.85	0.42
Camera Position (z) (meters)	0	-0.1	-0.05	-0.1	-0.02	0.09
Camera Pitch (degrees)	0	0	0	-1	0	1
Camera Yaw (degrees)	0	0	0	0	0	0
Vertical FoV (degrees)	42	45	44	42	45	45
RGB Resolution (H)	224	224	224	224	224	224
RGB Resolution (Y)	396	396	394	394	392	392
Rotation Center (x) (meters)	0	0.04	0.1	0.1	-0.02	-0.15
Rotation Center (z) (meters)	0	-0.13	0	0.13	0.02	-0.12
Collider Size (x) (meters)	0.35	0.27	0.36	0.37	0.27	0.42
Collider Size (y) (meters)	0.89	1.28	1.23	0.86	1.46	0.59
Collider Size (z) (meters)scale z	0.4	0.43	0.23	0.36	0.36	0.45
distance	-	0.18	0.22	0.34	0.41	0.42

Table 11. Five Nearest Neighbor Embodiments for LoCoBot in Training Data.

	Unitree A1	Nearest Neighbors				
		N1	N2	N3	N4	N5
Camera Position (x) (meters)	0.01	0.08	0.03	-0.01	-0.04	0.1
Camera Position (y) (meters)	0.3	0.56	0.37	0.85	0.55	0.82
Camera Position (z) (meters)	0.27	-0.11	0.06	0	0.12	0.02
Camera Pitch (degrees)	0	-3	-2	-4	-5	-5
Camera Yaw (degrees)	0	0	0	0	0	0
Vertical FoV (degrees)	42	49	49	51	50	51
RGB Resolution (H)	270	224	224	224	224	224
RGB Resolution (Y)	480	448	446	448	446	446
Rotation Center (x) (meters)	0	-0.07	0.05	-0.07	-0.09	-0.14
Rotation Center (z) (meters)	0.04	-0.02	0	-0.12	0.12	0.11
Collider Size (x) (meters)	0.3	0.46	0.27	0.35	0.27	0.49
Collider Size (y) (meters)	0.34	1.24	0.45	1.47	0.67	1.39
Collider Size (z) (meters)	0.64	0.34	0.37	0.36	0.33	0.39
distance	-	0.76	0.78	1.04	1.1	1.12

Table 12. Five Nearest Neighbor Embodiments for Unitree A1 in Training Data.

10. Nearest Neighbor Embodiments to Real Robots in our Training Data

Fig. 13 presents a t-SNE visualization of the embodiment parameters $\mathbf{c}_e \in \mathbb{R}^{19}$ for 50k samples from the random embodiments in our training set (examples shown in Fig. 14). We also show the corresponding parameters for Stretch, LoCoBot, and Unitree A1 for visualization purposes. Our random embodiments range widely over the space of possible embodiments, with many closely approximating each of the three real robots. Tables 10, 11, and 12 list the five nearest neighbors to each robot in the compressed t-SNE space and



Figure 14. **Random embodiments in the AI2-THOR simulator.** Right column shows the egocentric view from the main camera and the left column shows a third-person view of the agent –white boxes indicate the robot colliders for visualization purposes only.

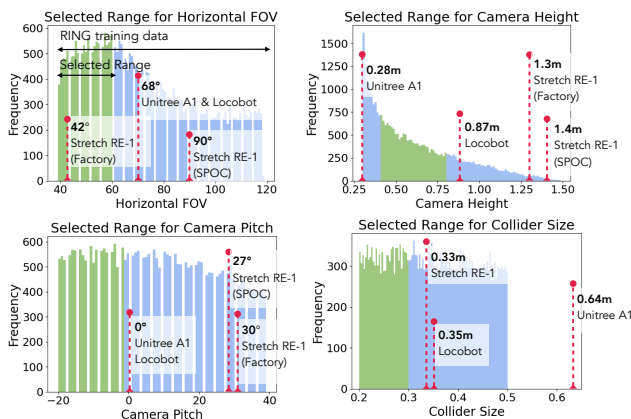


Figure 15. **Selected training ranges for the four embodiment parameters (camera height, camera FOV, camera pitch, and collider size).** The green regions represent the narrower ranges used during training, excluding the values corresponding to the real robots. The results of policies trained on each selected range are presented in Table 13.

their corresponding embodiment parameters. Although the nearest neighbors do not exactly match each robot’s embodiment, they are sufficiently similar across different parameters. This extensive coverage of the embodiment space and proximity to real-world embodiments ensure consistent zero-shot generalization to all three robots.

11. Generalization to out-of-distribution embodiment parameters

The random embodiments in our training set span a wide range of possible configurations, with many closely approximating each of the three real robots. Although the training data covers the full range of each embodiment parameter individually, the specific combination of parameters corresponding to each real robot is not explicitly included. This is demonstrated by the nearest-neighbor embodiments shown in Appendix 10. In this section, we examine the ex-

tent to which the policy generalizes to out-of-distribution values of individual embodiment parameters.

We focus on four specific parameters: camera height, camera field of view (FOV), camera pitch, and collider size. For each parameter, we define a narrower range that excludes the values corresponding to the real robots. From the training data, we filter the random embodiments to select 50k samples within each of these specified ranges. For comparison, we also train a version of the policy using 50k unfiltered embodiments that span the full range of each parameter. The selected training ranges for each parameter are illustrated in Fig. 15.

We then perform zero-shot evaluations of the policies trained on each selected range using four robots whose parameters lie outside the training ranges. The success rate and collision rate are summarized in Table 13. The results indicate that policies trained on narrower ranges still generalize to out-of-distribution parameters, achieving only a slightly lower success rate. However, evaluation on unseen embodiment parameters leads to a significantly higher collision rate, particularly for the policy trained with a narrower range of collider sizes. This suggests that the agent may rely more on physical contact with the environment to infer its embodiment configurations. Comparing Table 13 and Table 2, the average success rate drops by 13%, emphasizing that the number of random embodiments used during training is crucial to develop an embodiment-agnostic policy capable of effectively handling a wide range of embodiments.

12. Limitations

Although RING has the advantage of being deployable on a wide range of embodiments without any privileged information about its current body, when available it may be beneficial to have a policy explicitly conditioned on the current embodiment specification. This might lead to improved performance and more desirable behaviors, such as increased efficiency and collision avoidance.

We train RING-EMB-COND by explicitly providing the

Embodiment Parameter	Training Range	Success Rate↑ / Collision Rate ↓				
		Stretch	Stretch (Factory Config)	LoCoBot	Unitree A1	Average
Camera Height	[0.4, 0.8]	55.3 / 9.3	51.0 / 9.8	51.5 / 9.8	59.3 / 9.2	54.3 / 9.5
Camera FoV	[40, 60]	54.0 / 14.3	51.6 / 15.5	53.4 / 12.8	61.5 / 11.5	55.1 / 13.5
Camera Pitch	[-20, -2]	54.5 / 12.9	53.5 / 9.7	56.5 / 11.2	59.8 / 12.7	56.1 / 11.6
Collider Size	[0.20, 0.32]	60.5 / 18.0	53.5 / 21.4	55.0 / 14.9	54.0 / 18.6	55.7 / 18.2
No Filter	-	58.8 / 9.6	60.0 / 9.5	56.5 / 7.9	60.9 / 8.3	59.1 / 8.8

Table 13. **Out-of-distribution (OOD) generalization for different embodiment parameters.** For each of the four embodiment parameters, we select 50k random embodiments from a narrow training range that excludes the parameter values of the real robots (as shown in Fig. 15). Zero-shot evaluations are performed on four real robots, each with parameter values outside the training distribution. Success and collision rates are reported for each robot and averaged across all robots.

embodiment information to the policy. The embodiment parameters are represented as a configuration vector $c_e \in \mathbb{R}^{19}$, with each dimension corresponding to a specific embodiment parameter listed in Table 1. This information is passed as an additional token to the Transformer State Encoder. We use a simple MLP to project c_e to the desired feature dimension $e \in \mathbb{R}^{1 \times 512}$ before passing it to the encoder.

Table 14 evaluates the 2 versions of the policy on our custom benchmark consisting of 2,000 random embodiments across 2,000 scenes, comparing metrics such as *Success Rate*, *Success Weighted by Collision (SC)*, *Collision Rate (CR)*, and *Safe Episode (percentage of episodes without any collisions)*.

The results do not show a clear benefit to conditioning the policy on embodiment information. This could be due to several reasons. It is possible that most relevant information about environment hazards and agent motion can be already inferred from visual observations. It is also possible that a significant fraction portion of collisions (both with an without embodiment specification provided) occur with objects that never enter the agent’s visual field, in which case extra information about its own embodiment would not help. Alternatively, a more effective method for conditioning the policy on the parameters may exist. Future work should explore this with additional examination of agent-environment collision and designing improved policy architectures to better integrate embodiment parameters, ultimately training a more efficient and robust policy that explicitly incorporates embodiment information.

Model	Ablations	Success ↑	SEL ↑	SC ↑	CR ↓	Safe Episode ↑
	Body Config					
RING	✗	67.62	56.24	42.53	7.77	46.90
RING-EMB-COND	✓	69.44	57.42	44.69	8.0	46.54

Table 14. **Conditioning RING on embodiment parameters.** We explicitly provide the embodiment parameters to the policy (RING-EMB-COND) and compare with RING without any information about the embodiment. Both policies are evaluated on a custom benchmark consisting of 2000 random embodiments in 2000 scenes.